Discharge Characteristics of Composite Insulation System with Floating Electrode and Solid Insulator in Vacuum

Fei Kong, Yusuke Nakano, Hiroki Kojima, Naoki Hayakawa
Department of Electrical Engineering and Computer Science, Nagoya University
Furo-cho, Chikusa-ku, Nagoya, 464-8603, Japan

Toshinori Kimura and **Mitsuru Tsukima**
Mitsubishi Electric Corporation
Advanced Technology R&D Center
8-1-1, Tsukaguchi-honmachi, Amagasaki, 661-8661, Japan

ABSTRACT

For the development of vacuum interrupters for their higher voltage application in power transmission systems, it is necessary to clarify the discharge characteristics of composite insulation systems with a shield (floating electrode) and a solid insulator in vacuum. In this paper, we focus on the composite discharge patterns via the shield and the solid insulator. For cathode-shield-insulator-anode (c-s-i-a) and cathode-insulator-shield-anode (c-i-s-a) electrode configurations, the discharge can be classified into two independent processes: breakdown in vacuum gap and surface flashover on the solid insulator. Furthermore, we have found that the breakdown development time increases with the increase in the gap length and the surface flashover development time depends on the voltage peak after flashover inception, which are consistent with discharge development characteristics for individual gap breakdown and surface flashover, respectively. These results are significant to understanding and discriminating the composite discharge patterns and discharge path in vacuum interrupters.

Index Terms — **Vacuum, floating electrode, alumina ceramics, breakdown, surface flashover**

1 INTRODUCTION

VACUUM circuit breakers (VCBs) and vacuum interrupters (VIs) have many significant features such as simple structure, environment-friendliness, maintenance-free and so on. They have been utilized worldwide in medium voltage system and distribution power networks. Recently, VCBs/VIs are being developed for higher voltage application in order to substitute for SF_6 gas insulated switchgears and to help solve global warming problems [1-3]. Therefore, the enhancement of electrical insulation performance and the clarification of the fundamental discharge mechanism in vacuum are necessary.

The internal insulation problems in VI mainly exist between the main contacts, between a contact and a shield, and along a solid insulator, as shown in Figure 1. When the internal insulation fails in VI, as a composite insulation system, the discharge has complex patterns for various discharge sites and paths. References [4-6] show combined discharge patterns for the composite insulation system in VI, where the pattern classification and development characteristics of vacuum discharge have not been clarified enough.

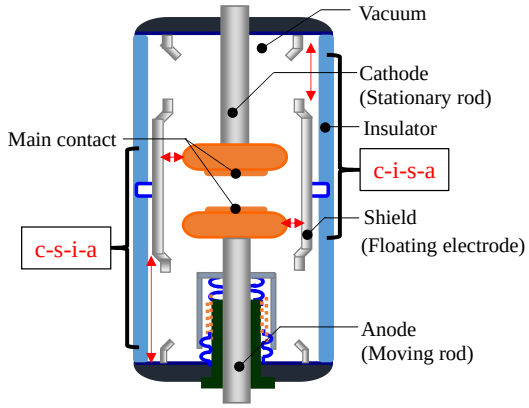

Figure 1. Composite discharge patterns in VI, when a stationary contact has a negative voltage to a moving contact.

We have been investigating the discharge characteristics for the breakdown in vacuum gap and the surface flashover on a solid insulator, respectively, and clarified the fundamental discharge development characteristics. In this paper, we focus on the discharge characteristics of composite insulation systems with both breakdown in vacuum gap and surface flashover on the solid insulator, which can contribute to the discrimination of discharge patterns of composite insulation

Manuscript received on X Month 2005, in final form XX Month 2005.

system in VIs. As shown in Figure 1, cathode-shield-insulator-anode (c-s-i-a) and cathode-insulator-shield-anode (c-i-s-a) represent the possible composite discharge patterns via the shield and the solid insulator. Correspondingly, composite electrode configurations were proposed and discharge pattern classification and development mechanisms were discussed.

2 EXPERIMENTAL SETUP

2.1 ELECTRODE CONFIGURATION

Figure 2 shows two kinds of electrode configuration to investigate the composite discharge patterns via a shield and a solid insulator. Figure 2a shows the electrode configuration simulating a path through a cathode-shield-insulator-anode (c-s-i-a) in VI. The cathode and the anode has a rod shape with a diameter of 2 mm, and is made of stainless steel. The shield is also made of stainless steel with dimensions of 120 mm × 60 mm × 2 mm^t. The floating electrode as a shield is placed on the insulator. The insulator is alumina ceramic (Al_2O_3, purity: 92%) with dimensions of 150 mm × 150 mm × 5 mm^t. The anode is in contact with the insulator surface. In addition, we set a grounded back electrode (70 mm × 20 mm) behind the insulator in order to control the discharge path. The vacuum gap length g between the cathode and the shield was set to 0.5 mm. The surface distance on the insulator from the shield edge to the anode is 60 mm.

Figure 2b shows the electrode configuration of a cathode-insulator-shield-anode (c-i-s-a), whose arrangement of insulator and the shield was changed from that in Figure 2a. The vacuum gap length g_1 between the cathode and the insulator was set to 0.5 mm. The vacuum gap length g_2 between the shield and the anode was set to 0.5 mm. The surface distance on the insulator below the cathode to the shield edge is 60 mm.

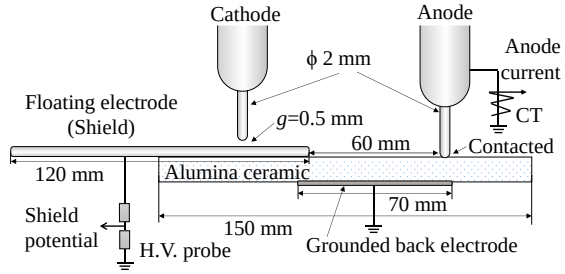

(a) Cathode-shield-insulator-anode (c-s-i-a)

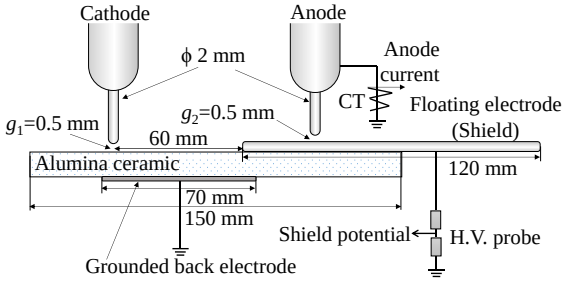

(b) Cathode- insulator-shield-anode (c-i-s-a)

Figure 2. Electrode configuration.

The average surface roughness of the alumina ceramic is 0.69 μm. Before the experiment, the alumina and electrodes were cleaned with ethanol and dried in vacuum for over 12 hours.

2.2 TEST CIRCUIT

Figure 3 shows the experimental setup with measurement systems. The vacuum pressure in the chamber is set to 10^{-5} Pa order. The impulse generator provides a negative standard lightning impulse voltage (1.2/50 μs). We applied the negative impulse voltage between the composite electrodes described in section 2.1 from the initial charging voltage of 10 kV with an increment of 2 kV. We carried out the voltage application more than 20 times for each electrode configuration.

We measured the applied voltage waveform with a voltage divider (1/45900), the anode current with a high frequency current transformer (CT, 1-20 MHz), and the shield potential with a high voltage probe (input impedance: 100 MΩ). These waveforms are acquired by a digital oscilloscope (2.5 GHz, 40 GS/s). In addition, still images of discharge were captured with a digital camera and the light intensity of discharge with a photomultiplier tube (PMT, 300-900 nm).

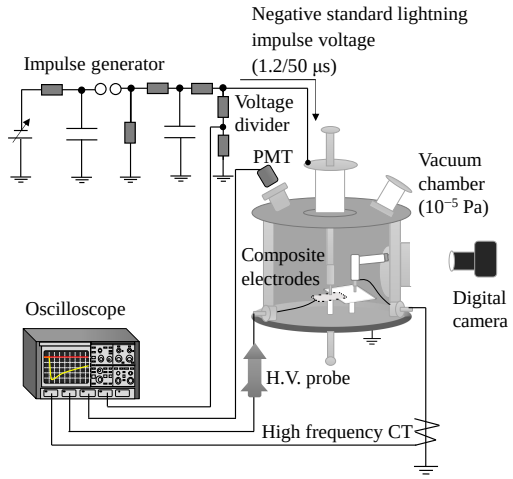

Figure 3. Experimental setup with measurement systems.

3 EXPRIMENTAL RESULTS AND DISCUSSION

3.1 DISCHARGE PROCESS BY WAY OF CATHODE-SHIELD-INSULATOR-ANODE (c-s-i-a)

In c-s-i-a electrode configuration, two discharge patterns were measured: partial breakdown (PB) as the gap discharge only between the cathode and the shield (c-s), and complete breakdown (BD) involving surface flashover along the insulator between the shield and the anode (c-s-i-a).

Figure 4 shows the discharge pattern of PB between the cathode and the shield whose potential difference ΔV at PB inception is −15.4 kV (applied voltage: V_a = −17.2 kV_{peak}). As shown in Figure 4a, weak light emission was observed only in the gap between the cathode and the shield. As shown in Figure 4b, the shield potential jumped up to the instantaneous cathode voltage, once PB occurred. The anode current was

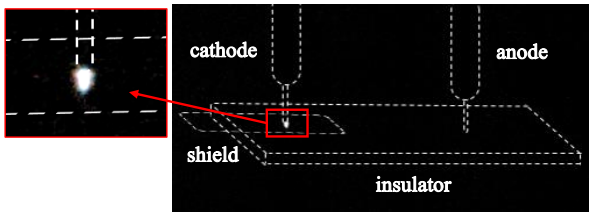

(a) Still image

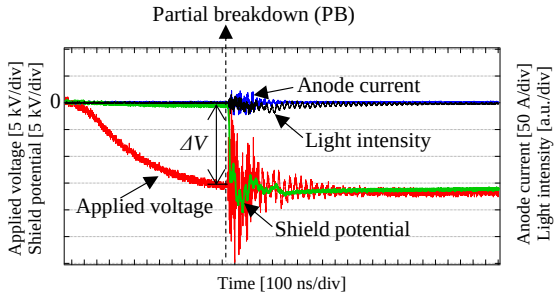

(b) Waveforms of applied voltage, shield potential, anode current and light intensity

Figure 4. Still image and discharge waveforms for partial breakdown in c-s-i-a electrode system (g = 0.5 mm, V_a = −17.2 kV_{peak}, ΔV = 15.4 kV).

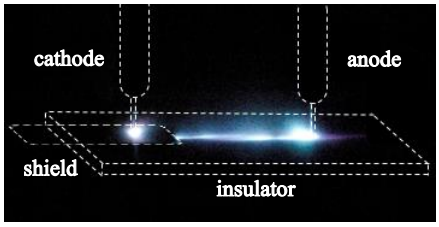

(a) Still image

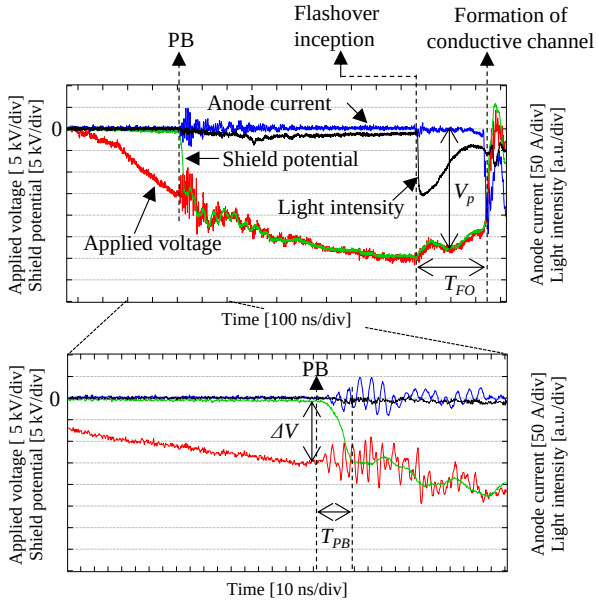

(b) Waveforms of applied voltage, shield potential, anode current and light intensity

Figure 5. Still image and discharge waveforms for case-1 in c-s-i-a breakdown (g = 0.5 mm, V_a = −32.7 kV_{peak}, ΔV = 14.4 kV).
T_{PB}: PB development time i.e. rise time of shield potential
T_{FO}: surface flashover development time from flashover inception to formation of conductive channel
V_p: voltage peak after surface flashover inception

almost zero, because no discharge channel was formed on the insulator surface between the shield and the anode (s-a).

In the case of higher voltage application, complete BD involving the surface flashover along the insulator occurred. For c-s-i-a BD, two cases (case-1 and case-2) could be distinguished by the discharge waveforms, as shown in Figures 5 and 6.

Figure 5 shows the still image and discharge waveforms for case-1 in c-s-i-a BD (V_a = −32.7 kV_{peak}). As shown in Figure 5a, light emissions both in the vacuum gap between the cathode and the shield and on the insulator surface could be observed. Figure 5b shows the discharge process for case-1 in c-s-i-a BD. After PB between the cathode and the shield, the shield potential jumped up to the instantaneous applied voltage, as well as in Figure 4b. By keeping the PB, the shield potential increased with the applied voltage. Afterwards, the surface flashover began to propagate between the shield and the insulator (s-i) with explosive electron emission (EEE) at the shield [7], then the applied voltage and the shield potential started to decrease. Finally, due to the formation of a conductive channel between the shield and the anode, the applied voltage and the shield potential decreased to almost 0 V and the anode current exceeded 100 A which was limited by the impendence of the test circuit.

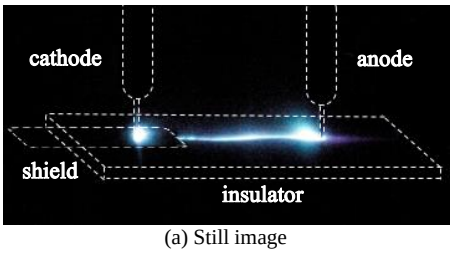

(a) Still image

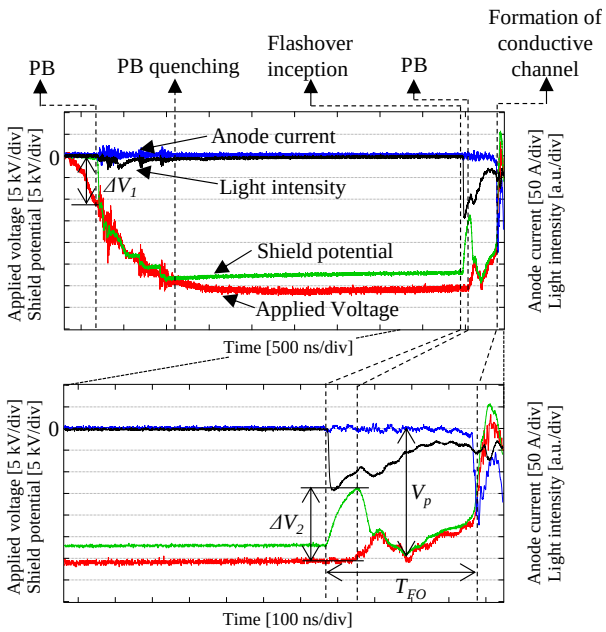

(b) Waveforms of applied voltage, shield potential, anode current and light intensity.

Figure 6. Still image and discharge waveforms for case-2 in c-s-i-a breakdown (g = 0.5 mm, V_a = −31.8 kV_{peak}, ΔV_1 = 11.1 kV, ΔV_2 = 16.6 kV).
ΔV_1 and ΔV_2: potential difference between the cathode and the shield at PB inception

Figure 6 shows the still image and discharge waveforms for case-2 in c-s-i-a BD (V_a = −31.8 kV_{peak}). Unlike in case-1, after the PB between the cathode and the shield, the shield potential remained a constant value, though the applied voltage continued to increase. This is because that the PB was quenched and the shield was floated again before the flashover initiation, which might be due to the unstable cathode spot [8]. At 3.4 μs after the PB quenching, the surface flashover between the shield and the anode occurred and developed to the anode, which resulted in a decrease in the shield potential. The time delay of 3.4 μs may be attributed to the statistical phenomena of EEE inception at the shield edge. Due to the increase in potential difference between the cathode and the shield, PB occurred again. Hence, the shield potential jumped up to the instantaneous applied voltage one more time. Finally, in the same way as those in case-1, due to the formation of a conductive channel along the insulator, the applied voltage and shield potential decreased to almost 0 V.

3.2 DISCHARGE PROCESS BY WAY OF CATHODE-INSULATOR- SHIELD-ANODE (c-i-s-a)

In c-i-s-a electrode configuration, two discharge patterns were measured: surface flashover (FO) between cathode and shield (c-i-s), and complete breakdown (BD) involving breakdown between shield and anode (c-i-s-a).

Figure 7 shows the still image and discharge waveforms for the surface flashover between cathode and shield via insulator (c-i-s) (V_a = −24.9 kV_{peak}). In Figure 7a, intense light emission near the cathode tip was confirmed and weak light emission was observed on the insulator surface between the cathode and the shield. As shown in Figure 7b, the surface flashover started with EEE at the cathode. Since the surface flashover developed toward the shield, the shield potential increased due to negative charging. The applied voltage began to decrease with the increase in the shield potential, nevertheless the discharge channel between the shield and the anode was not formed. This may be due to the discharge propagation from the charged shield.

In the case of higher voltage application, the complete BD of c-i-s-a occurred. For this pattern, due to the difference in the discharge inception between the shield and the anode depending on the shield surface condition and its potential, three cases (case-1, case-2, and case-3) were found by the timing of breakdown occurrence between the shield and the anode, as shown in Figures 8-10.

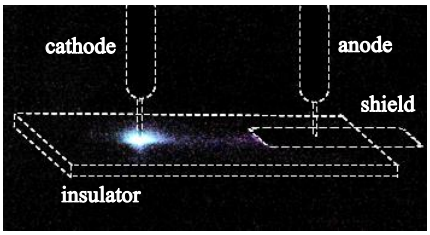

(a) Still image

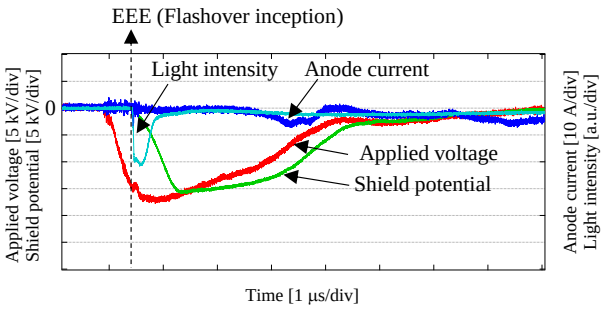

(b) Waveforms of applied voltage, shield potential, anode current and light intensity

Figure 7. Still image and discharge waveforms for c-i-s flashover in c-i-s-a electrode system (g_2 = 0.5 mm, V_a = −24.9 kV_{peak}).

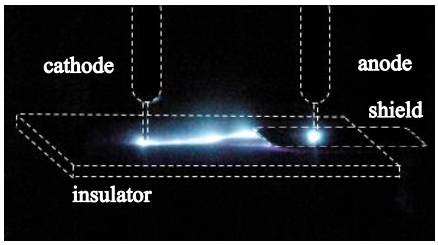

(a) Still image

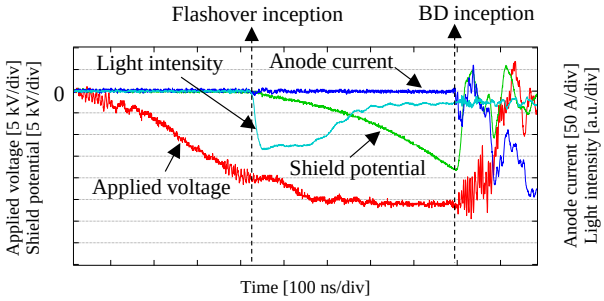

(b) Waveforms of applied voltage, shield potential, anode current and light intensity

Figure 8. Still image and discharge waveforms for case-1 in c-i-s-a BD (g_2 = 0.5 mm, V_a = −44.7 kV_{peak}).

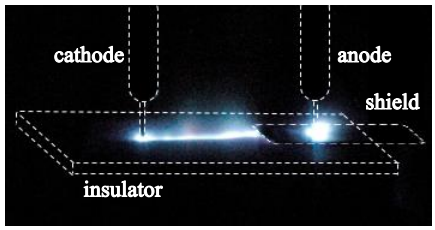

(a) Still image

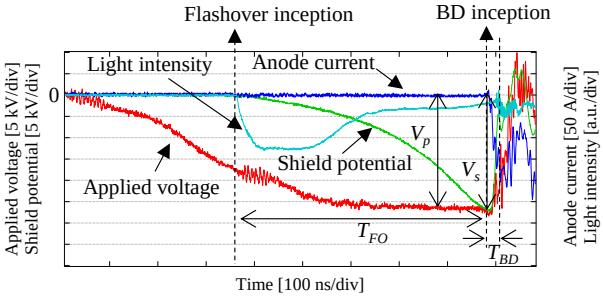

(b) Waveforms of applied voltage, shield potential, anode current and light intensity

Figure 9. Still image and discharge waveforms for case-2 in c-i-s-a BD (g_2 = 0.5 mm, V_a = −48.1 kV_{peak}).
T_{FO}: surface flashover development time from flashover inception between cathode and shield to the shield potential increase up to the cathode voltage
T_{BD}: BD development time i.e. fall time of shield potential
V_p: voltage peak after surface flashover inception
V_s: shield potential at BD inception

Figure 8 shows the still image and discharge waveforms for case-1 in c-i-s-a BD (V_a = −44.7 kV_{peak}). In Figure 8a, light emissions both on the insulator and in the vacuum gap between shield and anode were observed. Figure 8b shows the discharge waveforms for case-1 in c-i-s-a BD. Before the shield potential reached the applied voltage, discharge between the shield and the anode occurred. Figure 9 shows case-2 in c-i-s-a BD. When the shield potential reached the applied voltage, discharge between the shield and the anode occurred. In case-3 as shown in Figure 10, at 280 ns after the shield potential reached the applied voltage, discharge between the shield and the anode occurred.

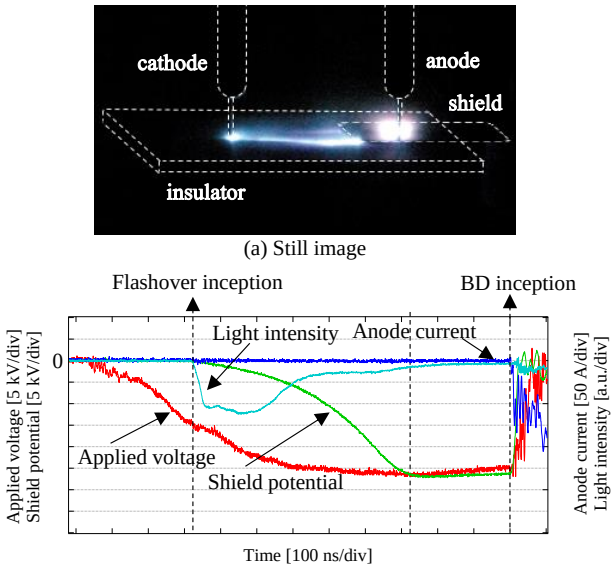

(a) Still image

(b) Waveforms of applied voltage, shield potential, anode current and light intensity

Figure 10. Still image and discharge waveforms for case-3 in c-i-s-a BD (g_2 = 0.5 mm, V_a = −46.4 kV_{peak}).

3.3 DISCUSSION ON DISCHARGE DEVELOPMENT CHARACTRISTICS

For the above results of two electrode configurations (c-s-i-a, c-i-s-a) in Figure 2, the discharge can be classified into two processes: breakdown in vacuum gap and surface flashover on the solid insulator. Here, by comparison with the individual discharge process, we discuss the discharge development characteristics for breakdown in vacuum gap and surface flashover on the solid insulator, respectively.

3.3.1 Breakdown characteristics in vacuum gap

Firstly, we focus on the discharge inception between the cathode and the shield. Figure 11 shows the potential differences between the cathode and the shield at the first PB (ΔV_1 in Figure 6) and at the PB after flashover inception (ΔV_2 in Figure 6). The error bar represents the maximum and minimum values of ΔV_1 and ΔV_2. Though ΔV_1 and ΔV_2 have a relatively large scattering, a significant or substantial difference cannot be found between ΔV_1 and ΔV_2. Thus, the occurrence of discharge between the cathode and the shield can be independent of the onset of surface discharge between the shield and the anode.

Next, in order to discuss the discharge development characteristics for breakdown in vacuum gap, we defined the rise time of shield potential as PB development time T_{PB} as shown in Figure 5b, and the fall time of shield potential as BD development time T_{BD} in Figure 9b, respectively. Figure 12 shows T_{PB} at various potential difference ΔV between the cathode and the shield in Figure 5b and T_{BD} at various shield potential V_s when BD occurred between the shield and the anode in Figure 9b. Since both cases mean breakdown in vacuum gap with the gap length of 0.5 mm, ΔV and V_s represent potential difference in the vacuum gap at breakdown inception. The average breakdown development time T_{PB} and T_{BD} are 32 ns, irrespective of ΔV and V_s. In these periods, cathode plasma can be produced at the cathode or shield surface and expand to the anode [9]. The cathode plasma expansion velocity is calculated to be in the order of 10^4 m/s,

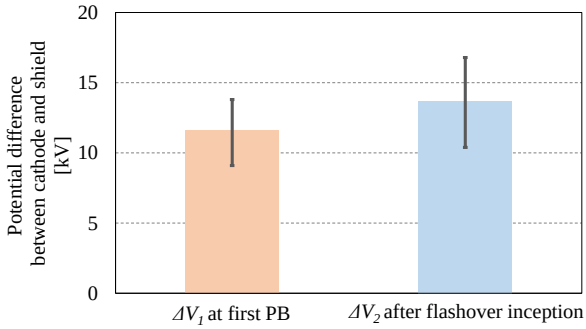

Figure 11. Potential difference between cathode and shield for case-2 in c-s-i-a BD.

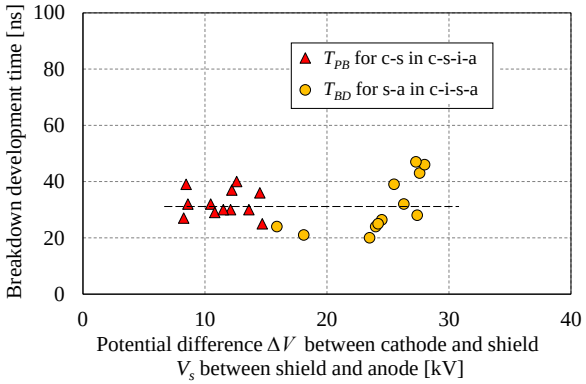

Figure 12. Breakdown development time T_{PB} at various potential difference ΔV between cathode and shield and T_{BD} at various shield potential V_s between shield and anode for vacuum gap discharge at gap length of 0.5 mm

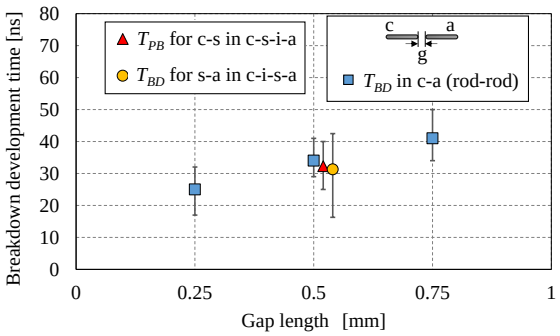

Figure 13. Breakdown development time characteristics for c-s in c-s-i-a, s-a in c-i-s-a, and c-a in rod-rod electrode configuration.

which is determined by the electrode material, and independent of the potential difference between the cathode and the shield, i.e. electric field strength [10, 11]. Figure 13 shows the breakdown development time for c-s in c-s-i-a, s-a in c-i-s-a at the gap length of 0.5 mm, together with our preliminary results for c-a in rod-rod electrodes at the gap lengths of 0.25-0.75 mm. At a gap length of 0.5 mm, T_{PB} in c-s-i-a and T_{BD} in c-i-s-a are consistent with the BD development time in c-a (rod-rod), which suggests the independence of the electrode configuration.

3.3.2 Surface flashover characteristics

In our preliminary experiments, we also investigated the surface flashover development characteristics on the solid insulator for cathode-insulator-anode (c-i-a), and found that T_{FO} is proportional to V_p^{-2} based on the electron-stimulated outgassing model [12]. According to this model, after surface flashover inception, with electron-stimulated outgassing from the insulator, the plasma density above the insulator surface increases with gaseous ionization, and eventually leads to the formation of a conductive channel [13-15]. The electron-stimulated outgassing can be promoted with higher voltage, which makes a shorter T_{FO}. For the parallel plane electrode configuration, the electron-stimulated outgassing depends on the electric field E_y on the insulator surface perpendicular to the insulator which is produced by charge on the insulator surface, and T_{FO} is proportional to E_y^{-2} [13]. On the other hand, in our electrode configuration, E_y is mainly decided by the applied voltage, i.e. V_p. Hence, T_{FO} is proportional to V_p^{-2} also in our electrode configuration.

Here, as shown in Figure 5b, we define the time from the flashover inception between s-i to the formation of a conductive channel as the surface flashover development time T_{FO}. In Figure 9b, we define the time from the flashover inception between c-i to the shield potential increase up to the cathode voltage as the surface flashover development time T_{FO}. In addition, we define the voltage peak after the surface flashover inception as V_p. As shown in Figure 14, the surface flashover development time T_{FO} for c-s-i-a in Figure 5b and c-i-s-a in Figure 9b are consistent with the surface flashover for c-i-a configuration.

In summary, for the composite insulation system with floating electrode and solid insulator, the composite discharge patterns can be regarded as the combination of vacuum gap breakdown and surface flashover, whose discharge characteristics are consistent with those in the individual discharge processes. These results and discussions are expected to be useful to understand the discharge patterns and path in vacuum interrupters with composite insulation system.

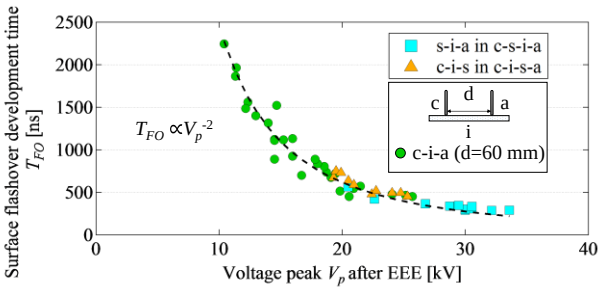

Figure 14. Surface flashover development time characteristics for s-i-a in c-s-i-a electrode configuration, c-i-s in c-i-s-a electrode configuration, and c-i-a electrode configuration.

4 CONCLUSION

Through the measurement and analysis of discharge waveforms (applied voltage, anode current and shield potential), we investigated the discharge characteristics of composite discharge patterns in vacuum.

The main results are summarized as follows:

(1) In both of the cathode-shield-insulator-anode (c-s-i-a) and cathode-insulator-shield-anode (c-i-s-a) electrode configurations, discharge waveforms enable us to classify two independent discharge patterns: breakdown in vacuum gap and surface flashover on the solid insulator.

(2) For the partial breakdown (PB) between cathode and shield in c-s-i-a BD, the occurrence of PB is independent of the onset of surface discharge. The PB development time T_{PB} does not depend on the potential difference between cathode and shield.

(3) The discharge development characteristics in composite discharge patterns are consistent with the individual discharge patterns. In the breakdown development process, the breakdown development time increases with the increase in the gap length. In the surface flashover development process, the surface flashover development time is inversely proportional to the square of voltage peak V_p after the surface flashover inception.

These discharge characteristics are significant to understand the discharge patterns and discharge path when an insulation failure occurs in the composite insulation system of vacuum interrupters. These results will contribute to the identification of the insulation weak points in vacuum interrupters as well as contribute to advanced and reliable insulation design of vacuum circuit breakers.

REFERENCES

[1] L. T. Falkingham, "Vacuum Interrupter Design for HV and VHV Applications", the 22nd International Symposium on Discharges and Electrical Insulation in Vacuum, pp.204-207, 2006.

[2] H. Okubo, H. Kojima, K. Kato, N. Hayakawa and M. Hanai, "Advanced Electrical Insulation Techniques for Higher Voltage Vacuum Interrupters", CIGRE B3/D1 Colloquium, No.218 (2013).

[3] M. Kamarol, S. Ohtsuka, M.Hikita, H.Saitou and M. Sakaki, "Determination of Gas Pressure in Vacuum Interrupter Based on Partial Discharge", IEEE Transactions on Dielectrics and Electrical Insulation, Vol.14, No.3, pp.593-599, 2007.

[4] H. C. Miller, "Electrical Discharge in Vacuum 1980-1990", IEEE Transactions on Electrical Insulation, Vol.26, No.5, pp.949-1043, 1991.

[5] V. A. Nevrovsky and L. A. Rylskaya, "Limiting Electric Strength of Vacuum Electrode Systems Including Combined Breakdown", the 20th International Symposium on Discharges and Electrical Insulation in Vacuum, pp.190-193, 2002.

[6] Irina N. Poluyanovo, Vladimir A. Bugayov and Anton V. Vykhodtsev, "Voltage Shape of Impulse Breakdown in Internal Insulation of VI", the 26th International Symposium on Discharges and Electrical Insulation in Vacuum, pp.441-444, 2014.

[7] Y. Nakano, H. Kojima, N. Hayakawa, K. Tsuchiya and H. Okubo, “Pre-discharge and Flashover Characteristics of Impulse Surface Discharge in Vacuum”, IEEE Transactions on Dielectrics and Electrical Insulation, Vol.21, No.1, pp.403-410, 2014.
[8] S. A. Barengolts, G. A. Mesyats and D. L. Shmelev, “Structure and Time Behavior of Vacuum Arc Cathode Spots”, IEEE Transactions on Plasma Science, Vol.31, No.5, pp.809-816, October, 2003.
[9] Gennady A. Mesyats and D. I. Proskurovsky, “Pulsed Electrical Discharge in Vacuum”, 1st ed., Springer-Verlag, pp.118-135, 1989.
[10] E. Hantzsche, “Theory of the Expanding Plasma of Vacuum Arcs”, J.Phys.D: Applied Physics, Vol.24, pp.1339-1353, 1991.
[11] Isak I. Beilis, “State of the Theory of Vacuum Arcs”, IEEE Transactions on Plasma Science, Vol.29, No.5, pp.657-670, October, 2001.
[12] F. Kong, Y. Nakano, H. Kojima, T. Kimura, M. Tsukima, and N. Hayakawa, “Conductive Channel Formation Time in Surface Flashover Development Process in Vacuum”, 2015 Annual Meeting of IEEJ, 1-117, 2015 (in Japanese).
[13] R. A. Anderson and J. P. Brainard, “Mechanism of Pulsed Surface Flashover Involving Electron-stimulated Desorption”, Journal of Applied Physics, Vol.51, No.3, pp.1414-1421, 1980.
[14] A. Sivathanu Pillai and Reuben Hackam, “Surface Flashover of Solid Dielectric in Vacuum”, Journal of Applied Physics, Vol.53, No.4, pp.2983-2987, 1982.
[15] Andreas A. Neuber, M. Butcher, H. Krompholz, Lynn L. Hatfield and Magne Kristiansen, “The Role of Outgassing in Surface Flashover under Vacuum”, IEEE Transactions on Plasma Science, Vol.28, No.5, pp.1593-1598, 2000.

Fei Kong (S’14) was born on 13 July in 1987. He received the M.S. degree in electrical engineering from Beijing Jiaotong University, Beijing, China, in 2011. Currently, he is a Ph.D. candidate of Nagoya University (MEXT scholarship) at the Department of Electrical Engineering and Computer Science. His major research interests include discharges phenomenon and electrical insulation in vacuum. He is a member of IEE of Japan.

Yusuke Nakano (S’12−M’15) was born on 5 March in 1988. He received the Ph.D. degree in 2015 in electrical engineering from Nagoya University. He received ICEPE-ST Wang Jimei Best Paper Award in 2013. His major research interests include surface flashover and electrical insulation in vacuum. Dr. Nakano is a member of IEE of Japan.

Hiroki Kojima (M’11) was born on 7 December 1975. He received the Ph.D. degree in 2004 in energy engineering and science from Nagoya University. Since 2004, he has been at Nagoya University and presently he is an Associate Professor of Nagoya University at the Department of Electrical Engineering and Computer Science. Dr. Kojima is a member of IEE of Japan.

Naoki Hayakawa (M’90) was born on 9 September 1962. He received the Ph.D. degree in 1991 in electrical engineering from Nagoya University. Since 1990, he has been at Nagoya University and presently he is a Professor of Nagoya University at the Department of Electrical Engineering and Computer Science. From 2001 to 2002, he was a guest scientist at the Forschungszentrum Karlsruhe/Germany. Prof. Hayakawa is a member of CIGRE and IEE of Japan.

Toshinori Kimura was born in Japan on June 27, 1964. He received the B.S. and M.S. degrees in physics from Hokkaido University in 1988 and 1990, respectively. In 1990, he joined Mitsubishi Electric Corporation. Presently, he is engaged in researching arc physics and the development of vacuum circuit breakers in Advanced Technology R&D Center. Mr. Kimura is a member of IEE of Japan.

Mitsuru Tsukima was born in Kyoto, Japan, on June 2, 1970. He received the B.S. and M.S. degrees in applied physics from Osaka University, Osaka, Japan, in 1994 and 1996, respectively. He joined the Advanced Technology R&D Center, Mitsubishi Electric Corporation, Amagasaki, Japan, in 1996. He is currently working on circuit breakers and related technologies. Dr. Tsukima is a member of IEE of Japan.